Original Paper

Predicted and measured glass surface temperatures in an industrial, regeneratively gas-fired flat glass furnace

R. Robert Hayes, Jian Wang, Mardson Q. McQuay and Brent W. Webb
Mechanical Engineering Department, Brigham Young University, Provo, UT (USA)

Aaron M. Huber
Ford Motor Company Glass Division, Dearborn, MI (USA)

This study reports optically measured glass surface temperatures along the furnace center-line in the combustion space of a side-port, 455 (metric) t/d industrial, gas-fired flat glass furnace. The measurements were made using a water-cooled two-color pyrometer inserted through holes in the crown at six locations along the length of the furnace. Both average and time-resolved glass surface temperature measurements were performed during the approximately 20 s reversal period of the furnace. The measured glass surface temperature data are supplemented by observations of the batch location using a specially designed, water-cooled video probe. The average temperatures were found to rise from a low near 1700 K near the batch blanket to a peak of approximately 1900 K, then drop to a level of 1800 K. Evidence of batch islands or "logs" is observed in the surface temperature data collected at the measurement location nearest the batch blanket. Large temperature excursions are seen here, indicative of measurement alternately of both the batch surface and the molten glass. Also reported in this study are results of a numerical model for the three-dimensional melt flow and heat transfer in the tank, coupled with a batch melting model. The radiant heat flux distribution incident on the melt and batch blanket surfaces is assumed. The melt tank model includes bubbling. The numerical predictions agree well with the time-averaged glass surface temperature data collected experimentally. The measurements and model predictions illustrate the complex transport phenomena in the melting section of the furnace.

Vorausgesagte und gemessene Glasoberflächentemperaturen in einer industriellen, regenerativ gasbeheizten Flachglaswanne

Der Beitrag berichtet über Glasoberflächentemperaturen, die im Verbrennungsraum einer industriellen gasbeheizten Querbrennerwanne zur Herstellung von Flachglas (455 t/d) entlang der Ofenmittellinie optisch gemessen wurden. Die Messungen wurden mit Hilfe eines wassergekühlten Zweifarbenpyrometers gemacht, das an sechs Stellen längs des Wannengewölbes durch Löcher eingeführt wurde. Während der Wechselperiode von 20 s wurden Messungen sowohl der durchschnittlichen als auch der zeitlich aufgelösten Glasoberflächentemperaturen durchgeführt. Die gemessenen Daten werden durch Beobachtungen der Lage des Gemenges mit Hilfe einer speziell gefertigten, wassergekühlten Videosonde ergänzt. Die Durchschnittstemperaturen steigen vom einem tiefsten Punkt bei ungefähr 1700 K in der Nähe des Gemengeteppichs zu einer Höhe von ungefähr 1900 K und fallen dann auf ein Niveau von 1800 K. Die Oberflächentemperaturwerte, die bei dem Meßort, der dem Gemengeteppich am nächsten liegt, gewonnen wurden, geben Anhaltspunkte für die Existenz von Gemengeinseln oder "logs". Große Temperaturunterschiede werden hier festgestellt, die zeigen, daß abwechselnd die Gemengeoberfläche und das geschmolzene Glas gemessen wurden. Außerdem werden die Ergebnisse eines numerischen Modells des dreidimensionalen Schmelzflusses und der Wärmeübertragung in der Wanne (gekoppelt mit einem Modell des Gemengeschmelzens) wiedergegeben. Die auf die Schmelze und die Oberfläche des Gemengeteppichs auftreffende Strahlungswärmeflußverteilung wird geschätzt. Das Glasschmelzwannen-Modell berücksichtigt den Vorgang des Bubbling. Die numerischen Voraussagen stimmen gut mit den experimentell gewonnenen, zeitlich gemittelten Glasoberflächen-Temperaturdaten überein. Die Messungen und die Modellvoraussagen zeigen die komplexen Transportvorgänge im Schmelzbereich der Wanne.

1. Introduction

The design of modern industrial combustion furnaces has become increasingly important from both environmental and economic standpoints. The competing objectives of high efficiency and low emissions have created a complex challenge. A better understanding of the combustion and other transport processes and the ability to model more accurately the combustion behavior are required to best meet these objectives. These challenges are certainly evident in the area of industrial glass furnaces. Modern design efforts increasingly rely on three-dimensional numerical models of the combustion space and glass melt tank. This trend is substantiated by the large number of recent publications in this field [1 to 31]. However, experimental data from industrial-scale glass furnaces are nearly nonexistent [32 to 37]. In addition to the important role that these measurements play in increasing the understanding of the melting and combustion processes, there is an immediate application for experimental data in the development and evaluation of numerical models created to predict the combustion,

Received 21 April, revised manuscript 14 September 1999.

batch melting, and melt circulation in these industrial furnaces. Important fundamental parameters for model validation and understanding of the combustion process include gas species composition, heat flux, gas temperature, gas velocity, wall temperature, and glass surface temperature.

The limited experimental data from industrial glass furnaces found in the open literature consist of only seven studies. Experimental measurements in an end-port, oil-fired, regenerative, container glass furnace with a nominal output of 90 t/d of soda-lime glass and a specific energy consumption of 5.9 GJ/t are reported by Cassiano et al. [33]. Two operating conditions were tested to investigate the effect of furnace throughput and air-fuel ratio on the heat transfer characteristics of the furnace. Local gas temperatures, wall incident radiant heat fluxes, and gas species concentrations were measured through six existing inspection ports in the furnace. Quantification of cyclic operation of the furnace as well as the three-dimensional nature of the combustion process are reported. No time-resolved information was reported and measurements through the crown of the furnace were not possible because of the lack of access ports in that region. Based on these measurements and modeling of the combustion process together with an on-line furnace viewing system, the implementation of a new furnace control scheme is also reported by Farmer et al. [34] and Victor et al. [35].

Experimental measurements were also reported for a similar end-port furnace with a nominal output of 160 t/d of amber glass and a specific energy consumption of 4.9 GJ/t [36]. Local gas temperatures and average gas species concentrations (O_2, CO, CO_2, and NO_x) were measured. These measurements were taken through three ports located on the side of the furnace. The cyclic operation of the furnace as well as the three-dimensional nature of the flow and combustion were characterized. No radiative fluxes, velocities, or time dependence studies of the regenerative furnace were reported.

Profiles of gas velocity, species concentrations (O_2, CO, and CO_2), average wall incident radiant heat flux, and gas temperature have recently been reported for the combustion space and exhaust ports of a regenerative, side-port, gas-fired, flat glass furnace with a nominal output of 455 t/d [30 and 32]. A region of fast-moving gases near the glass, with axial velocity components exceeding 20 m/s, and a large recirculation zone near the furnace crown have been reported based on gas velocity measurements. Temperatures as high as 1985 K in the flame and as low as 1750 K in the recirculation zone were reported. A zone of intense reaction near the glass, with large concentration gradients, and incomplete combustion were also observed. CO_2 concentrations were the highest near the batch, where the glass reactions are most intense. Local average incident radiant fluxes in the crown were spatially uniform at 680 kW/m^2. Significant variations were observed in the exhaust profiles of most measured variables. Large errors in exhaust mass balance suggest a complex, three-dimensional flow with recirculation zones along the side walls of the port necks. A nominal preheat air temperature of 1420 K and a variation in exhaust temperatures from port to port between 1630 K and 1835 K were reported. High O_2 concentrations, reaching 8.4 %, were measured in the exit, suggesting a bypass of oxygen-rich flow around the flame. Limited time-dependent measurements at a few locations were reported for some variables, including species concentration, gas velocity, and gas temperature. These transient measurements were restricted by the time-response of the instrumentation, and usually represent data points acquired at 2 to 3 min intervals over a 15 to 20 min period.

The most recent report was a study of this same furnace after it was rebuilt [37]. Post-rebuild profiles of velocity, species concentrations (O_2, CO, and CO_2) and gas temperature data are reported and compared with the pre-rebuild data measured previously in the same furnace. Additionally, measurements were also taken below one of the regenerators in the tunnel leading to the furnace stack. Fewer variations were observed in the exhaust profiles of most measured variables after the rebuild. Flat inlet velocity profiles were measured with an approximate magnitude of 11 m/s. Exhaust velocities after rebuild are reported to reach maximums of 21 m/s, compared with 26 m/s before rebuild. Exhaust gas temperatures were, generally speaking, higher in the post-rebuild furnace, while inlet preheated air temperatures were observed to be consistently lower after the rebuild. The locations of low O_2 concentration in the effluent were shown to be consistent with the high CO concentrations existing both before and after the rebuild. The measurements in the tunnel resulted in very low CO levels, indicating that the combustion reactions continue inside the regenerators resulting in overall complete combustion.

In the previously mentioned studies glass surface temperature measurements are not reported. The temperature of the glass surface inside the combustion space is a critical parameter for the understanding of the combustion and melt circulation processes, as well as validating numerical models. It is crucial to the understanding of the energy transfer to the glass, which is of primary interest in design considerations. Additionally, the glass surface temperature plays an important role in determining the quality of the glass being produced.

The objective of the experimental study reported here is to measure, for the first time, the temperature of the glass surface in the combustion space of an industrial, gas-fired, flat glass furnace. In addition, the measurements reported are time-resolved, to investigate transient phenomena during the 20 s reversal period, when firing does not take place. The data are obtained in a regenerative, side-port, 455 t/d gas-fired flat glass furnace owned and operated by Ford Motor Company Glass Division in Tulsa, OK (USA) [30 and 32 and 37]. The data presented are unique. The measurements were

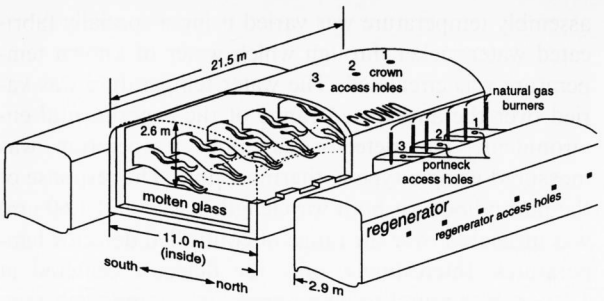

Figure 1. Schematic (not drawn to scale) of the side-port, 455 t/d, gas-fired, flat glass furnace where measurements were made.

obtained through six access holes in the crown of the furnace. The information obtained includes average temperature of the glass surface at each of the six port locations, as well as time-resolved information at five of the port locations, all measured during reversal of the regenerator cycle. Additionally, a numerical model of the batch melting and glass tank is developed and presented to support the analysis of the measured data and enhance the overall understanding of the physical phenomena involved. Furthermore, glass surface temperature data and the numerical glass tank model results are compared with visual information that provides glass surface and batch blanket locations.

2. Experimental procedure and instrumentation

A schematic of the glass furnace can be seen in figure 1. The furnace is approximately 2.6 m high from the glass line to the maximum height of the crown, 11 m wide, and 21.5 m long. A regenerator is located on the north and south sides of the furnace. Connecting each regenerator and the furnace is a set of six portnecks approximately 2.9 m long. At the regenerator opening each portneck is nominally 1.5 m wide and 1 m high. At the furnace inlet the height of each portneck narrows to 0.5 m and the width expands to 1.8 m. Each port has two 4.4-cm-diameter pipe burners located 81.3 cm from the edge of the furnace and 43.2 cm above the glass line. Each burner is angled so that the centerline of the flow will intersect the portneck centerline at the edge of the furnace. The furnace operates on a 15 min cycle: a 15 min burn from the north portnecks with exhaust through the south (identified here as north/south configuration or firing direction), a reversal period (approximately 20 s) during which no firing occurs, followed by 15 min in the opposite direction (i.e., south/north configuration or firing direction). The furnace was constructed with six thermo-couple plugs used to measure the crown temperature. These plugs, when removed, provided access holes located along the center of the crown apex at axial furnace locations coinciding with the transverse centerlines of each of the six ports (see figure 1).

The total combustion fuel flow rates, airflow rates, and firing stoichiometry for each port during furnace operation are shown in table 1. The fuel flow rates presented were measured by the plant during operation when the measurements presented were performed. The inlet airflow rates shown were not measured, but were calculated for each port. Using the measured fuel flow rates and previously measured exhaust values of O_2 and CO_2 in each port, the combustion reaction equation was balanced for each port to solve for the inlet airflow rates [37]. As noted in this table, the majority of the fuel is distributed in ports nos. 1 to 5, with a smaller fraction used in the port nearest to the working end of the furnace (port no. 6).

Table 1. Furnace firing conditions in ports nos. 1 to 6.

port no.	fuel flow rate[1] in kg/h	air flow rate[2] in kg/h	excess air[3] in %
1	583	9 680	12
2	667	11 110	13
3	666	10 680	8
4	651	10 240	6
5	679	14 200	41
6	243	6 380	77

[1] Fuel flow rate for each port as reported by the plant.
[2] Air flow rates estimated using previously measured exhaust species compositions [37].
[3] Values calculated using total measured fuel flow rates and estimated air flow rates.

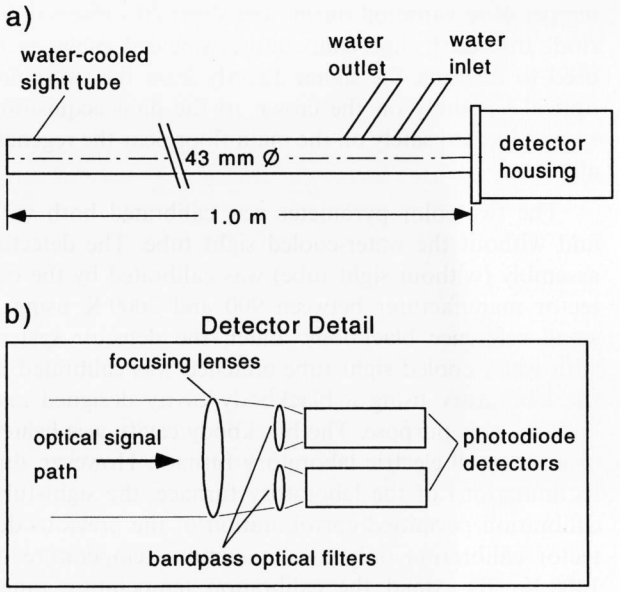

Figures 2a and b. Schematics of the two-color pyrometer instrument used for optical glass surface temperature measurements (figure a) and of the detector detail (figure b).

Glass surface temperatures were measured optically using a two-color pyrometer. Figures 2a and b are schematics of the instrument. The optical detector housing is mounted on a water-cooled sight tube. The sight tube is approximately 2.8 cm in inner diameter and 1.0 m long. Lenses, located in the optical detector housing, image the infrared radiation entering the sight tube onto amplified germanium photodiodes. The radiation is transmitted through interference filters with 30 nm

bandwidths centered at 1.27 and 1.60 μm. These wavelengths were chosen to avoid the absorption bands of CO_2 and water vapor. The signal amplification system for each channel was constructed with adjustable gain to permit modification for a range of high temperatures and a variety of data acquisition equipment.

For the glass temperature measurements the amplified output from the detector was between 1 and 12 V. Time-averaged readings were obtained using a voltmeter, while both time-averaged and time-resolved measurements were acquired and recorded using a computer-based data-acquisition system, with a 12-bit analog-to-digital converter. This system provided a sampling rate of 5000 Hz for temperature measurements, enabling a thorough time-resolved investigation of the glass surface temperature variation during the short 20 s reversal period. Insulated, high-temperature, shielded cables were used to transmit the signal directly from the two-color optical assembly on the crown to the data acquisition system located safely on the main floor near the regenerator.

The two-color pyrometer was calibrated both with and without the water-cooled sight tube. The detector assembly (without sight tube) was calibrated by the detector manufacturer between 900 and 2000 K using a small reference blackbody. Later, the detector system with water-cooled sight tube attached was calibrated in the laboratory using a blackbody cavity designed and built for this purpose. The blackbody cavity was heated using a small electric laboratory furnace. However, due to limitations of the laboratory furnace, the sight-tube calibration permitted corroboration of the previous detector calibration only to a maximum temperature of 1400 K. To extend the calibration temperature range with the attached sight tube, a torch-heated ceramic-plate heat source was constructed. Aluminum oxide ceramic material (Coors AD 96; 96 Al_2O_3) was selected for its radiatively gray behavior over the range of the two wavelengths used by the pyrometer. A Type S (Pt-Pt10%Rh) thermocouple was inserted in a blind hole drilled into each side of the 6 mm thick ceramic plate, and an acetylene torch was used to heat the rear face while the optical pyrometer imaged the front face. The ceramic plate was heated to approximately 2000 K. An analysis was developed to estimate the front-face temperature from the measured internal temperature. The sight-tube calibration using the blackbody cavity (up to 1400 K) and the ceramic-plate heat source (up to 2000 K) enabled the detector assembly to be properly aligned with the sight tube, and confirmed the detector-only calibration performed previously to a temperature of 2000 K.

Exploratory measurements with the two-color pyrometer revealed the response of the photodiode/amplifier components to be somewhat ambient temperature-dependent. Laboratory experiments were performed to quantify this dependence. With a given blackbody source temperature, the two-color pyrometer detector assembly temperature was varied using a specially fabricated water jacket through which water of known temperature was circulated. The water temperature was varied over the anticipated range of the experimental environment. The detector assembly temperature was measured using a type K thermocouple. The response of the photodiodes at both wavelengths (1.27 and 1.60 μm) was measured over the range of controlled detector temperatures. Interestingly, only the detector centered at 1.60 μm was found to have appreciable component temperature-dependent response. A mathematical relation was formulated which accurately represents the temperature dependence of the amplifier sensitivity, and was included in the pyrometer calibration. During testing in the glass furnace environment, the detector assembly was cooled using vortex tube coolers with adjustable flow rate in order to minimize the temperature excursions. Additionally, the temperature of the detector assembly was measured and documented for later use in data reduction. A statistical analysis of all calibration data including the temperature dependence of the detectors reveals an estimated uncertainty in measured surface temperatures of ±30 K.

The photodiodes in the two-color pyrometer are designed to output an amplified voltage proportional to the emissive power incident on the detector. Using Wien's approximation to Planck's blackbody function, the heated surface temperature can be related to the ratio of the two wavelengths chosen for use, and the ratio of the photodiode voltages (and hence, the emissive powers) at the two wavelengths:

$$T = \frac{C_2(1/\lambda_2 - 1/\lambda_1)}{\ln[(V_{\lambda_1}/b)/V_{\lambda_2}] + 5\ln(\lambda_2/\lambda_1) + a} \quad (1)$$

where λ_1 and λ_2 are the two wavelengths chosen, V_{λ_1} and V_{λ_2} are the measured photodiode voltages at the two wavelengths, and C_2 is Planck's second fundamental radiation constant with a value of 1.44 10^7 nm K. The parameters a and b are calibration constants which account for first) the proportionality between photodiode voltage output and the incident emissive power (a), and second) the ambient temperature sensitivity of the 1.60 μm detector (b). Both constants were determined from experiments in the laboratory prior to the glass furnace measurements. The expression for Wien's approximation included these calibration constants, determined from exhaustive calibration data taken over the full range of blackbody and ceramic heat source temperatures (900 to 2000 K) and detector body temperatures (13 to 45 °C). The calibration relates the measured voltage from both detectors and the detector body temperature to the imaged surface temperature.

There are two physical phenomena which might affect the accuracy of the surface temperature measurements made using two-color pyrometry. First, the technique assumes that the surface is radiatively gray, i.e., that the spectral emissivity of the glass surface is iden-

tical at the two wavelengths used. Although the spectral emissivity was not measured for the gray glass being produced during the testing, previous work has shown that the assumption of gray behavior is valid, particularly over such a narrow wavelength range [38]. Second, glass is a semitransparent medium, with emission possibly originating from a layer of glass instead of the surface alone. Recently, measurements of the spectral absorption coefficient for several different types of glasses have been reported [39 to 41]. Based on these data it can be determined that the spectral optical thickness (product of the absorption coefficient and the layer physical thickness) for the melt layer imaged in the measurements reported here was in the order of 400. Thus, emission from the glass originated from a layer less than 1 cm thick. Therefore, it can be safely assumed that the temperature measurements reported are those of the glass surface.

Surface temperature measurements with the two-color pyrometer were taken in each of the six crown access holes, with location no. 1 being nearest to the batch feed and continuing through location no. 6, nearest to the working end of the furnace. Data were acquired during the reversal of the 15 min regenerator cycle, when all of the burners are off for approximately 20 s. This enabled the unobstructed (no flame) measurement of the molten glass surface below. The estimated optical view of the two-color detector at the glass surface was a circular area approximately 9 cm in diameter. Detailed time-resolved measurements were obtained for all crown access holes, with the exception of location no. 2, where only average surface temperature data was taken.

3. Numerical model

The batch melting and the flow and heat transfer in the glass melt were simulated using a glass tank model coupled in an integrated fashion with a batch melting model. The glass batch, which is fed into the tank by the batch feeder, floats on the surface of the molten glass to form a batch blanket. The batch material is then heated from the top surface radiatively from the combustion chamber and heated from the bottom surface by heat transfer from hot molten glass underneath. The batch melting model used was a quasi-three-dimensional mathematical model, which consisted of a series of thermally unconnected, two-dimensional "lanes" extending from the batch feeder in the direction of the furnace working end. Batch inlet velocities from the feeder were calculated according to the pull rate of the tank. The model included variation in the batch inlet velocity profile along the width of the tank entrance based upon the batch feeder configuration and tank entrance characteristics. This batch inlet velocity profile variation across the feeder at the tank entrance is important in obtaining an accurate prediction for the shape of the batch surface coverage. The temperature field, the melting process, the shape of the batch blanket and batch coverage area on the melt surface can be predicted by the batch model.

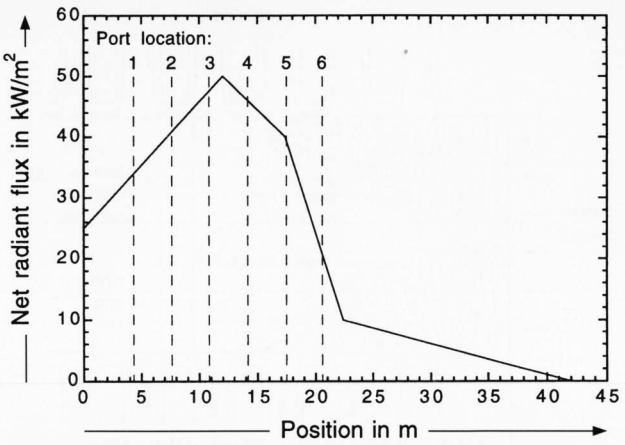

Figure 3. Axial profile of net heat flux on the batch/glass surface imposed as boundary conditions in the numerical simulations.

The glass melt is heated by radiant heat flux from the combustion space incident on the free surface of molten glass and cooled by the heat transfer to the batch blanket. It was assumed that the molten glass behaves as an incompressible Newtonian viscous fluid and that the flow and heat transfer inside the glass melt are at steady state. The volumetric radiation transfer inside the glass melt was handled using an effective thermal conductivity in the energy equation [24]. The coupled partial differential equations governing three-dimensional momentum and energy transport in the melt tank were solved using the control volume approach. Pressure coupling was handled using the SIMPLER algorithm [42]. This calculation procedure is followed until the convergence criteria (residuals smaller than 0.001) are met. The temperature field and velocity field in the molten glass are predicted by the glass tank model.

The glass tank model and batch melting model communicate with each other in an iterative fashion through the coupling procedure, matched by the relation between the heat flux from the molten glass to the bottom surface of the batch blanket and the melting mass flux from the batch blanket to the glass surface. The interface temperature and batch mass melting distribution are iteratively calculated. Further details regarding both the batch melting model and the glass tank model, as well as model coupling procedure, are described elsewhere [31].

Much of the required input information for the numerical model was obtained from furnace operating conditions. The pull rate of the furnace was 455 t/d of glass. The batch is fed into the tank from the doghouse located at the back wall. For the batch, raw materials constitute 65 % by weight and 35 % cullet by weight. The batch inlet temperature is 30 °C and the inlet thickness is 0.2 m. The thermal conductivity of the tank refractory walls and bottom were considered as 2.0 and 0.7 W/(m K), respectively. Boundary conditions used for the heat flux incident on the batch/glass surface were estimated according to the numerical results of a full combustion chamber model and furnace measurement experience [30, 32 and 37]. The

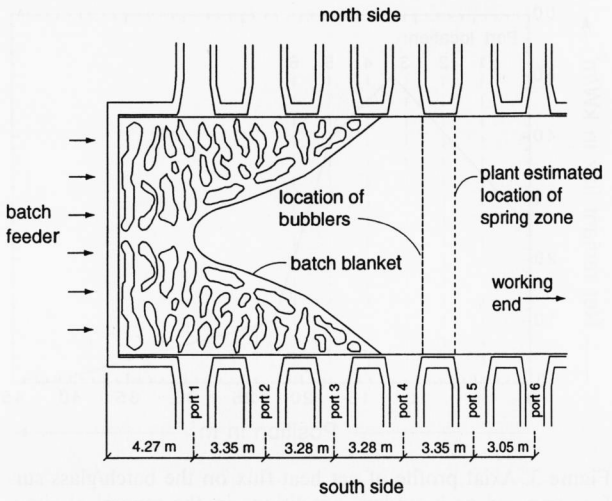

Figure 4. Schematic (plan view) of glass surface in the furnace based on information obtained from specialized video data and visual observations through furnace inspection ports, indicating bubbler location and estimated spring zone position.

boundary conditions imposed for net heat flux on the batch/glass surface are shown, along with port centerline locations in figure 3. The sensitivity of the predicted melt flow and temperature to the imposed heat flux was also investigated with the model by scaling the radiant heat flux profile shown in figure 3 by +10 % and −10 %, respectively. The computational grid used in the simulation was 195 000 cells (156 × 50 × 25) for the tank model and 264 000 cells (150 × 44 × 40) for the batch model, respectively. An HP workstation was used for the coupled model calculation, and converged results were obtained after approximately 8000 iterations. Two different cases were considered. One case included bubbler operation in the glass tank, as occurred during the period when the experimental measurements were acquired, while the other case did not include the operation of bubblers.

4. Discussion of results

This section presents and discusses the experimental results and numerical predictions. Initially, the complex physical phenomena are briefly discussed, as revealed through independently acquired video data and furnace operating information, to enhance and support the discussion of the experimental and modeling results that follows. Next, the measured average glass surface temperature data in all six of the crown access holes along the lengthwise centerline of the furnace are reported and discussed, together with the results of the three-dimensional numerical model of the glass tank and batch melting processes. Lastly, time-resolved glass surface temperature data are presented and discussed.

5. Physical phenomena

Figure 4 shows a schematic (plan view) of the glass surface from the furnace batch feeder wall to the end of port no. 6 with respect to the general characteristics of the furnace, such as the location of the six portnecks and the batch feeder. This schematic was constructed from video observations made through the crown access holes, visual observations made through other access ports constructed for visual inspection in the furnace which are located in the regenerators (along the centerline of the portnecks), and in the working end of the furnace looking toward the batch feeder. The video data obtained, delineating the brighter areas of molten glass and the much darker areas of batch blanket, were acquired using a high-resolution video camera with specialized filtered lenses attached to a water-cooled sight tube inserted through the crown access holes. The video probe apparatus allowed for a field of view of approximately 30 degrees, which provided clear information in the central region of the tank (2 to 2.5 m wide at the glass surface), but limited observations near the tank edges. Figure 4 also indicates additional information about characteristics of the glass tank: (a) the location of bubblers, which are used to enhance mixing of the molten glass, and (b) the approximate location of the "spring zone," where recirculating molten glass rises to the surface, causing the glass surface temperature to reach maximum values in the tank.

As illustrated in figure 4, the batch blanket profile shows that the surface boundary between the batch blanket and molten glass along the furnace axial centerline was located in the vicinity of location no. 1, approximately 4.3 m from the end wall closest to the batch feeder. The schematic also indicates that batch material was nonexistent along the furnace centerline past location no. 1, but extended along the sides of the furnace in the approximate profile shown, tapering in thickness along the furnace side walls until complete batch melt-out, which typically occurs in the vicinity of locations nos. 3 or 4. As expected, the surface boundary between batch and molten glass is not completely steady. The location of the batch blanket varies slightly during furnace operation with several factors influencing its movement. The batch material is introduced intermittently to the furnace because of the operating characteristics of the batch feeder, causing the batch material to exit the feeder and enter the furnace in discrete clumps or "logs." In addition, the molten glass recirculation pattern and batch melting contribute to batch movement at the surface near the batch blanket/glass interface. Lateral movement of the batch blanket was also visually observed, with the unmelted batch blanket tending to shift cyclically with firing direction. This cyclic surface motion was observed to be toward the exit port side during firing, returning slightly more to the center during reversal, then shifting to the opposite port side as firing begins in that direction. These factors were identified as contributors to batch blanket movement during furnace operation and to the intermittent existence of "batch islands," discrete smaller sections of batch material found near the boundary between the batch blanket and molten glass. The transient nature of the surface bound-

ary between batch blanket and molten glass was clearly established, although quantitative details of the contributing phenomena and specifics of their observed transient effects were not thoroughly studied.

Gases are liberated during the melting and chemical reaction which occurs as the raw materials from the batch are processed. This is particularly true in the early regions of the furnace where melting is most intense. The generation of gases in the melt results in bubbles which rise and accumulate on the surface as foam. Foam was observed only near the boundary separating the batch blanket from the batch-free zone downstream in the melting section. Thus, foam was observed intermittently near location no. 1, but all subsequent holes (locations nos. 2 to 6) where surface temperature measurement data were collected were unobstructed by foam.

6. Experimental results and model predictions

Glass surface temperatures measured at locations nos. 1 to 6, averaged over the 20 s reversal period, are shown in figure 5. The lowest average surface temperature measured was 1711 K at location no. 1, nearest the batch feeder. The average temperature then rises sharply from 1711 to 1853 K between locations nos. 1 and 2, continues to gradually rise to the peak measured temperatures of 1912 K at location no. 4 and 1910 K at location no. 5, and then falls to approximately 1804 K at location no. 6, nearest to the furnace working end.

Model predictions of the centerline glass-surface temperature profile with and without bubblers are also shown in figure 5. Although significant differences throughout the glass tank were apparent in the model results with and without bubblers, as will be shown and discussed later, the differences in the predicted glass surface temperature profiles along the furnace axial centerline between the two simulations were relatively small. The effects of bubbler operation on glass temperature predictions were much more significant in the lower regions of the glass tank near the bubblers.

The numerical model results presented were obtained under the assumption of steady state flow and heat transfer, as explained previously in the model description. Therefore, model results are compared with time-averaged experimental data. The model predictions agree well with both the qualitative profile and magnitudes of the measured average surface temperatures along the centerline of the furnace at all locations. The difference between model-predicted values and measured values at each location is always less than 45 K, with the average absolute difference being less than 20 K. The largest differences occur in the regions of highest temperature at locations nos. 4 and 5. Predictions made for the imposed radiant heat flux profile of figure 3 scaled by +10 % and −10 % (without bubblers) resulted in glass surface temperatures approximately 40 K above and below the base case prediction. The increased/decreased heat flux on the batch/melt has the effect of shifting the predicted glass surface temperature profile higher or lower, but the general profile shape remains the same.

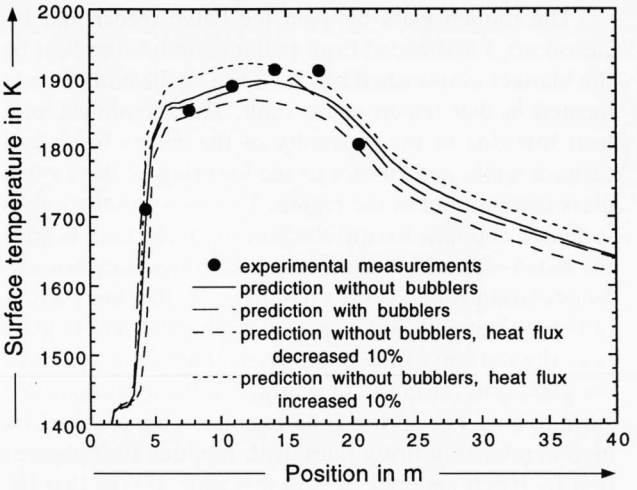

Figure 5. Comparison of measured and predicted average glass surface temperature profile along the furnace axial centerline in the glass tank.

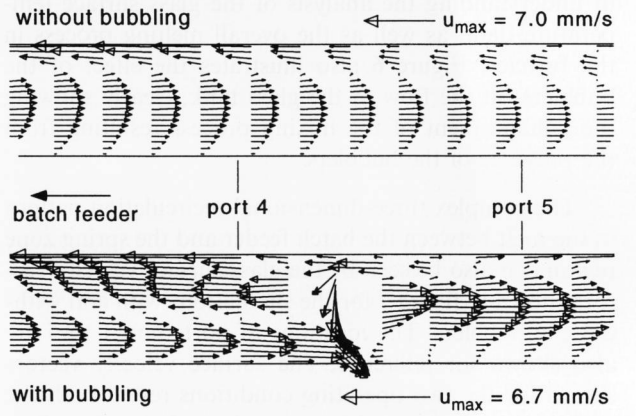

Figure 6. Velocity vector plots from the glass tank numerical model with and without bubblers in a vertical plane in the tank along the furnace axial centerline.

The numerical model also predicts two complex, buoyancy-driven, three-dimensional recirculation patterns in the molten glass tank. One is in the region between the spring zone and the batch feeder, the other between the working end and the spring zone. Figure 6 shows the predicted velocity vectors in the molten glass, for cases with and without the bubblers, in a vertical plane along the glass tank axial centerline. The magnified view of the predicted melt velocities near the spring zone, which is straddled by ports nos. 4 and 5, is shown. Although the simulations were performed for the entire glass tank, only the region near the spring zone is shown in figure 6 because of the importance of its effect on the surface temperatures measured. The position of these plots with respect to physical characteristics of the furnace is also included in this figure for clarity.

The molten glass between the batch feeder and location no. 1 is shielded from radiant combustion heat by the blanket of unmelted batch on top of the molten glass located in that region of the tank. This, combined with heat loss due to the proximity of the cooler batch and furnace walls, contributes to the lowering of the molten glass temperature in the region. The cooler molten glass is denser and falls toward the bottom of the tank nearest the batch-side tank wall, creating this three-dimensional, recirculation zone. As shown in figure 6, the flow pattern of the molten glass indicates that the higher-density glass near the bottom of the tank travels toward the center of the glass tank, rising to the surface at the location of the spring zone. The spring-zone region is characterized by high combustion firing rates, with minimal heat absorption by batch material. It is in this general area that the highest glass surface temperatures were measured. At the glass surface upstream of the spring zone, glass flows back toward the batch feed area. Downstream of the spring zone glass flows toward the furnace working end. The recirculation and glass flow patterns are important in understanding the analysis of the glass surface temperature data, as well as the overall melting process in the furnace. Figure 6 also illustrates the effect of the bubblers on the flow in the glass tank, clearly showing the enhancement of the mixing process resulting from the presence of the bubblers.

The complex three-dimensional recirculation pattern in the melt between the batch feeder and the spring zone region can also be seen by the glass surface velocity vectors shown in figure 7 for the simulations with and without the bubblers. The locations of ports nos. 1 to 5 are also shown for reference. The surface velocity vectors shown for the two operating conditions reveal both the predicted spring zone location, where the surface flow velocities are divided in opposite directions, and the predicted surface location of the batch blanket, where the velocity magnitudes arc significantly smaller than those on the molten glass surface. The region of large changes in surface velocity magnitudes outlines the predicted boundary between the molten glass and batch, where the high reverse surface velocities are rapidly decelerated. The location of the spring zone is shown in the figure to be approximately two-thirds of the way down the melting section, where the rising melt separates at the surface in the region between locations nos. 4 and 5. The differences in surface velocities between the two simulated cases appear to be relatively minor, with the simulation without bubblers exhibiting less variation in surface velocity laterally across the furnace for a given axial location. The effect of operation with the bubblers appears to result in a more curved surface velocity profile near the spring zone, with higher velocities near the furnace axial centerline and lower velocities angled away from the centerline in regions closest to the tank sides.

The trend in the measured average glass surface temperatures shown in figure 5 is consistent and in good agreement with the model predictions shown in the same

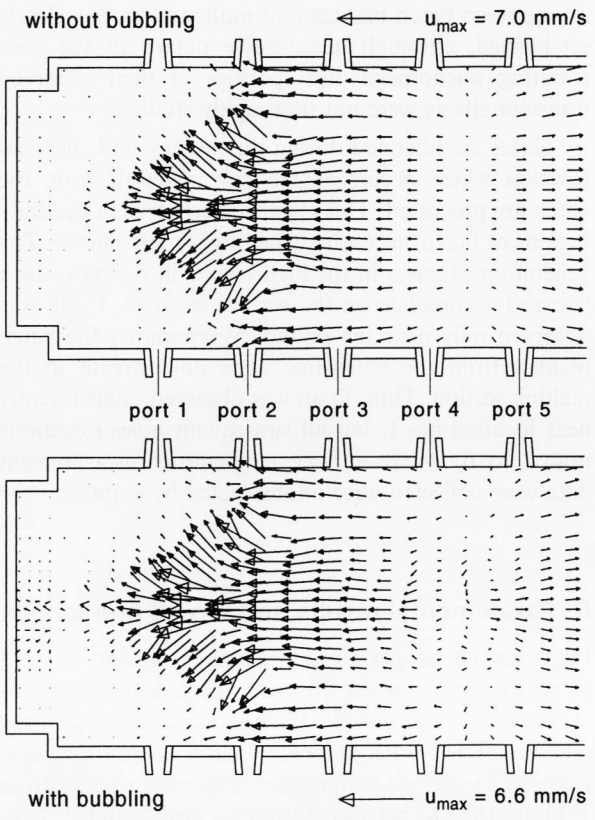

Figure 7. Surface velocity vector plots from the glass tank numerical model with and without bubblers.

figure, as well as the video and visual observations presented in figure 4. The low average glass surface temperature measured at location no. 1 is caused by the fact that this location is at the boundary of the cooler batch and the molten glass in a region where heat loss from the glass to the batch as well as to the tank walls is large. As will be discussed later in conjunction with the time-resolved surface temperature data, both molten glass and batch material were viewed and measured intermittently at location no. 1. As one moves away from this region where batch and molten glass coexist, a sharp increase in the average measured glass surface temperature is observed along the furnace centerline between locations nos. 1 and 2. In addition to the higher radiant heat flux received from the flame, location no. 2 being approximately 3.4 m further downstream of location no. 1 experiences less heat loss to the end wall and batch material. As one continues to approach the spring zone, the measured average glass temperature continues to increase gradually between locations nos. 2 and 3. This is confirmed by the numerical model predictions. The higher measured surface temperature at location no. 3 is due to a combination of factors, including: a) the recirculation flow pattern which feeds hotter molten glass from the spring zone into that region, b) the increase in firing rate and reduction of the overall excess air in the flame, and c) lower heat loss to the furnace end wall and to the ever-decreasing batch material along the tank edges.

As expected, the highest average glass surface temperatures measured were at locations nos. 4 and 5 in the region of the spring zone. These peak temperatures were due to the combined effects of the recirculation pattern in the glass tank, the minimum heat loss from the glass to batch or end walls, and the highest firing rates and lowest excess air values in the flames of ports nos. 4 and 5. Repeated measurements obtained at these locations showed that the average surface temperature magnitudes measured during different reversal periods varied less than 76 K at location no. 4, which is closest to the operating bubblers, and less than 20 K at location no. 5.

At location no. 6 the average measured glass surface temperature is much lower than temperatures measured at locations nos. 4 and 5. Although there is essentially no heat loss to the batch at location no. 6, there is additional heat loss to the cooler working end of the furnace where the glass exits. Location no. 6 also experiences considerably less heat transfer from the combustion products than do the other measured locations, due to the reduced firing in this port with significantly higher excess air (77 %). Thus the molten glass surface in this region experiences additional heat loss and the corresponding surface temperature drops due to convection that results from the unique firing conditions existing in port no. 6. These factors combine to maintain the lower surface temperature at this final measured location.

7. Time-resolved experimental results

Time-resolved glass surface temperature data measured during approximately 20 s of the reversal period when the flame is off are shown in figure 8. Typical measurement traces are shown in the figure.

The surface temperature at location no. 1 is seen to vary between 1440 and 1850 K during one 20 s reversal period. The temperature begins relatively low (approximately 1600 K), then rises slowly to a high plateau near 1820 K. It then drops drastically over a period of about 8.5 s to below 1500 K before rising slowly again to another high plateau of 1840 K for the remainder of the reversal period. This low frequency, large temperature variation is consistent with what might be expected if portions of the cooler batch blanket traverse the optical view area of the two-color pyrometer for a short time as they shift position in the glass tank in the region of location no. 1. This batch motion arises from the phenomenon explained previously in the discussion of figure 4, as well as the reverse velocities decelerating at the batch boundary, as shown in figure 7. The higher temperature plateaus observed both before and after the lowest temperature interval are both relatively steady and consistent in magnitude with one another, suggesting the measurement of the molten glass surface temperature during these periods. The lower temperature intervals of the data trace are consistent with the measurement of the surface of cooler unmelted or partially melted batch which exists as a continuous blanket along the centerline

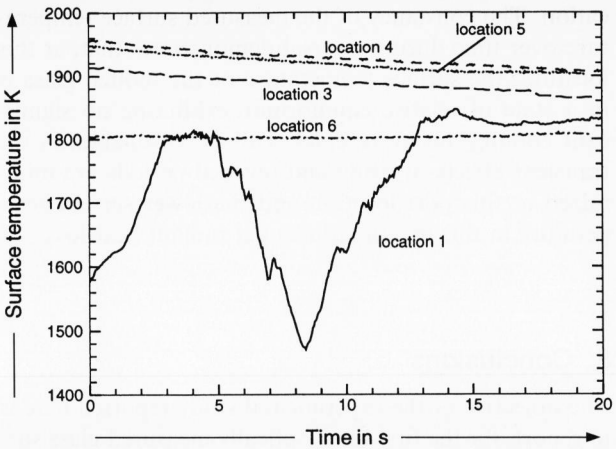

Figure 8. Typical time-resolved surface temperature plots acquired during reversal in locations nos. 1, 3, 4, 5 and 6.

of the tank from the batch feeder to location no. 1. It is not known if the intermittently measured batch surface is due to optically viewing the movement of the edge of the continuous batch blanket or moving batch islands that are pulled by molten glass currents. It is known, however, that the lower measured surface temperatures at location no. 1 are consistent with batch surface temperatures predicted by the model, and the visual observations and physical phenomena discussed previously. The time-resolved temperature signal measured in hole no. 1 is the only one to vary so widely during the reversal period. All other measured locations exhibit a more nearly constant surface temperature during reversal, because the surface temperature measurements at these locations are of molten glass only, with batch material being nonexistent along the axial centerline of the furnace downstream of location no. 1.

The time-resolved surface temperature measurements obtained at access locations nos. 3 to 6 indicate significantly less variation in molten glass surface temperature than at location no. 1. Locations nos. 3, 4 and 5 all have similar profiles, exhibiting a steady gradual surface temperature decline over the duration of the reversal period while the flame is not present. The data at these locations, shown in figure 8, thus illustrate the cooling of the molten glass surface during the brief nonfiring period. Nominally, the surface temperature is seen to drop 50 to 80 K over the no-flame reversal period. As would be expected, the slightly steeper decline in temperature takes place when surface temperatures are the highest, such as near the beginning of reversal at locations nos. 4 and 5, while the decline is more gradual when surface temperatures are lower.

The time-resolved temperature measurements of the glass surface at location no. 6, nearest to the glass tank exit, indicate a steady, nearly constant temperature profile that does not exhibit the same constant gradual decline as the other locations nos. 3 to 5. It is noted again that location no. 6 is unique in the combustion cycle process, as reduced air/fuel flow occurs at this port lo-

cation. The constancy of the measured surface temperature over time during reversal demonstrates that, at this location, the surface temperature of the molten glass is in a state of relative equilibrium, exhibiting no significant cooling during reversal. This is reasonable, as the transient effects of firing and reversal periods are minimized at this port location and the lower surface temperature in this region reduces net radiant heat loss.

8. Conclusions

The objective of the experimental study reported here is to report, for the first time, optically measured glass surface temperatures in the combustion space of an industrial, gas-fired, flat-glass furnace. Both average and time-resolved glass surface temperature measurements were performed during the approximately 20 s reversal period of a side-port, 455 t/d furnace.

The temperature measurements in the combustion space indicate that the average surface temperature profile rises sharply from a low near 1700 K closest to the batch feeder to about 1850 K at the next downstream location, then continues to rise steadily down the axial length of the furnace along the centerline to a peak of approximately 1910 K in the region of ports nos. 4 and 5. The molten glass surface temperature then drops to near 1800 K at the measured location closest to the furnace working end. The numerical predictions of glass surface temperatures agree well with the time-averaged experimental data at all measured locations, showing similar profile trends with differences in temperature magnitudes of less than 40 K at each location between the model and experimental results. The numerical model also reveals detail about the complex recirculating flow patterns in the tank. The model shows the area of highest glass surface temperatures, the spring zone, to be located between locations nos. 4 and 5, which is confirmed by the measured data and is also consistent with information obtained from plant personnel. In addition, the temperature measurements and model predictions are confirmed by video and visual observations of the glass surface during furnace operation.

The results of the time-resolved temperature data demonstrate that along the axial centerline of the combustion space, the surface boundary between batch material and molten glass exists in the immediate vicinity of location no. 1, nearest to the batch feeder. The data at this location reveal measured surface temperatures of both molten glass, near 1830 K, and much cooler batch material, near 1480 K. The time-resolved data also indicate that at downstream locations, a gradual cooling of the molten glass surface occurs during the 20 s nonfiring reversal period. The drop in temperature during this nonfiring interval is nominally in the range of 50 to 80 K. The measured glass surface temperature nearest to the furnace working end does not exhibit this same cooling and stays nearly constant over the reversal period.

*

Financial support of the U.S. Department of Energy through Agreement DE-FC02-95CE41187 and Ford Motor Company Glass Division is gratefully acknowledged. The DOE contract monitor is Mr. Edward Gallagher. Additional support of the National Science Foundation through the Advanced Combustion Engineering Research Center is also acknowledged. Ford Glass Plant support by Denny Fryz and Ken Traud is appreciated. The help and support by Todd Moss and Don Wallace of the Mechanical Engineering Department of Brigham Young University during equipment procurement and instrument calibration is also appreciated.

9. References

[1] Boerstoel, G. P.; Wieringa, J. A.; Meer, Th. H. van der: Numerical modeling of soot formation in glass melting furnaces. In: Heat Transfer in Radiating and Combusting Systems – 2. Proc. Eurotherm Seminar, No. 37 1994 p. 167–180.

[2] Boerstoel, G. P.; Meer, Th. H. van der; Hoogendoorn, C. J.: Numerical simulation of soot formation and oxidation in high temperature furnaces. In: Proc. ISTF-8, San Francisco, CA, 1995.

[3] Carvalho, M. G.; Lockwood, F. C.: Mathematical simulation of an end-port regenerative glass furnace. Proc. Inst. Mech. Eng. **199** (1985), p. 113–120.

[4] Carvalho, M. G.; Oliveira, P.; Semião, V.: A three-dimensional model of an industrial glass furnace. J. Inst. Energy **143**, (1988) p. 143–156.

[5] Carvalho, M. G.: Computer simulation of a glass furnace. University of London, Ph. D. thesis 1983.

[6] Carvalho, M. G.; Durão, D. F. G.; Pereira, J. C. F.: Prediction of the flow, reaction and heat transfer in an oxy-fuel glass furnace. Eng. Comput. **4** (1987) p. 23–34.

[7] Carvalho, M. G.; Semião, V.; Lockwood, F. C. et al.: Predictions of nitric oxide emissions from a industrial glass-melting furnace. J. Inst. Energy **63** (1990) p. 39–42.

[8] Carvalho, M. G.; Lockwood, F. C.: Thermal comparison of glass furnace operation with oil and natural gas. Glastech. Ber. **63** (1990) no. 9, p. 233–243.

[9] Carvalho, M. G.; Speranskaia, N.; Wang, J. et al.: Modeling of glass melting furnaces: Applications to control, design, and operation optimization. In: Clare, A. G.; Jones, L. E. (eds.): Advances in fusion and processing of glass II. Proc. 5th. Int. Conf. Advances Fusion Processing Glass, Toronto 1997. Westerville, OH: Am. Ceram. Soc., 1998. p. 109–135. (Ceram. Trans. Vol. 82.)

[10] Carvalho, M. G.; Wang, J.; Nogueira, M.: Physically-based numerical tool for the study of cleaner combustion in glass melting furnaces. In: Proc. IV International Conference on Technologies and Combustion for a Clean Environment, Lisbon 1997. Vol. II, p. 27.13–27.20.

[11] Carvalho, M. G.; Wang, J.; Nogueira, M.: Numerical simulation of thermal phenomena and particulate emissions in an industrial glass melting furnace. In: Fundamentals of glass science and technology 1997. Proc. 4th Conf. Eur. Soc. Glass Sci. Technol. Växjö 1997. Växjö: Glafo, 1997. p. 414–421.

[12] Carvalho, M. G.; Nogueira, M.; Wang, J. et al.: Model-based study of a glass melting furnace for reduced particle emission. In: Akçakaya, R.; Erinc, N.; Albayrak, G. et al. (eds.): Proc. International Symposium on Glass Problems, Istanbul, 1996. Vol. 1. Istanbul: Sisecam 1996. p. 398.

[13] Carvalho, M. G.; Nogueira, M.; Wang, J.: Assessment of numerical simulation of industrial glass melter. Verre **1** (1995) no. 5, p. 9–13.

[14] Carvalho, M. G.; Nogueira, M.; Wang, J.: Mathematical modeling of the glass melting industrial process. In: Proc. XVII International Congress on Glass, Beijing 1995. Vol. 6. Beijing: Chinese Ceram. Soc., 1995. p. 69–74.

[15] Chen, T.; Goodson, R. E.: Computation of three-dimensional temperature and convective flow profiles for an electric glass furnace. Glass Technol. **13** (1972) no. 6, p. 161–167.
[16] Gosman, A. D.; Lockwood, F. C.; Megahead, I. E. A. et al.: Prediction of the flow, reaction, and heat transfer in a glass furnace. J. Inst. Energy **6** (1982) p. 353–360.
[17] Gosman, A. D.; Lockwood, F. C.; Megahed, I. E. A.: The prediction of the flow, reaction, and heat transfer in the combustion chamber of a glass furnace. In: Proc. AIAA 18-Meeting on Aerospace Sciences, California, 1980.
[18] Mase, H.; Oda, K.: Mathematical model of glass tank furnace with batch melting process. J. Non-Cryst Solids **38** and **39** (1980) p. 807–812.
[19] McConnell, R. R.; Goodson, R. E.: Modelling of glass furnace design for improved energy efficiency. Glass Technol. **20** (1979) no. 3, 100–106.
[20] Megahed, I. E. A.: The prediction of three-dimensional gas-fired combustion chamber flows. University of London, Ph. D. thesis 1978.
[21] Novak, J. D.: Application of combustion space energy calculations to commercial glass furnaces. J. Non-Cryst Solids **38** and **39** (1980) p. 819–824.
[22] Post, L.: Modelling of flow and combustion in a glass melting furnace. Delft University of Technology, Ph. D. thesis 1988.
[23] Samião, V. S.: Numerical simulation in an industrial furnace. (Orig. Portug.) M. Sc. thesis, University of Lisbon, 1986.
[24] Wang, J.: Three-dimensional mathematical model of thermal phenomena occurring in industrial glass melting tanks. Instituto Superior Técnico, Lisbon Ph. D. thesis 1998.
[25] Wang, J.; Carvalho, M. G.: Model-based study of sand grain dissolution in industrial glass furnaces. In: Proc. 18th International Congress on Glass, San Francisco, CA 1998. (Available on CD Rom at Am. Ceram. Soc, Westerville, OH.)
[26] Wang, J.; Carvalho, M. G.; Nogueira, M.: An integrated methodology for glass furnace design. In: Proc. 18th International Congress on Glass, San Francisco, CA 1998. (Available on CD Rom at Am. Ceram. Soc, Westerville, OH.)
[27] Carvalho, M. G.; Wang, J.; Nogueira, M.: Investigation of Glass Melting and Fining Processes by Means of Comprehensive mathematical Model. In: Clare, A. G.; Jones, L. E. (eds.): Advances in fusion and processing of glass II. Proc. 5th Int. Conf. Advances Fusion Processing Glass, Toronto 1997. Westerville, OH: Am. Ceram. Soc., 1998. p. 143–152. (Ceram. Trans. Vol. 82)
[28] Wang, J.; Farias, T. L.; Carvalho, M. G. et al.: Radiation modeling procedures for numerical simulation of glass melting furnaces. In: Proc. IV. International Seminar on Mathematical Simulation in Glass Melting, Horni Bečva (Czech Republic) 1997. p. 10–20.
[29] Wang, J.; Carvalho, M. G.; Nogueira, M.: Physically-based numerical tool for the study of glass melt quality. In: Proc. 5th International Seminar on Mathematical Simulation in Glass Melting, Horni Bečva (Czech Republic) 1997. p. 67–76.
[30] Newbold, J. A.: Combustion measurements and modeling of an industrial, gas-fired, flat-glass furnace. Brigham Young University, Provo, UT M. S. thesis 1997.
[31] Wang, J.; Brewster, S.; Webb, B. W. et al.: A coupled combustion space/batch/melt tank model for an industrial float glass furnace. In: Proc. V International Seminar on Mathematical Simulation in Glass Melting, Horni Bečva (Czech Republic) 1999. p. 84–93.
[32] Newbold, J.; Webb, B. W.; McQuay, M. Q. et al.: Combustion measurements in an industrial gas-fired flat-glass furnace. J. Inst. Energy **70** (1997) p. 71–81.
[33] Cassiano, J.; Heitor, M. V.; Silva, T. F.: Combustion tests on an industrial glass-melting furnace. Fuel **73** (1994) p. 1638–1642.
[34] Farmer, D.; Heitor, M. V.; Sentiero, J. et al.: New methodology for furnace monitoring, analysis and control. Glass Ind. **73** (1992) no. 10, p. 10–12.
[35] Victor, A. S.; Costeira, J. P.; Tomé, J. A. et al.: A computer vision system for the characterization of flame in glass furnaces. In: Proc. IEEE Industry Applications Society Annual Meeting, Dearborn, MI 1991. p. 9/28–10/4.
[36] Costa, M.; Mourao, M.; Baltasar, J. et al.: Combustion measurements in an industrial glass melting furnace. J. Inst. Energy **69** (1996) p. 71–81.
[37] McQuay, M. Q.; Webb, B. W.: The effect of rebuild on the combustion performance of an industrial gas-fired flat glass furnace. Comb. Sci. Technol. (in press).
[38] Gardon, R.: A review of radiant heat transfer in glass. J. Am. Ceram. Soc. **44** (1961) no. 7, p. 305–317.
[39] Endrys, J.: Measurement of Radiative and Effective Thermal Conductivity of Glass. In: Proc. 5th Conf. European Society of Glass Science and Technology (ESG), Prague 1999. Vol. A5, p. 10–17.
[40] Nijnatten, P. A. van; Broekhuijse, J. T.; Faber, A. J.: Spectral photon conductivity of glass at forming and melting temperatures. In: Proc. 5th Conf. European Society of Glass Science and Technology (ESG), Prague 1999. Vol. A5, p. 2–9. (Available on CD-ROM.)
[41] Nijnatten, P. A. van; Broekhuijse, J. T.: A high-temperature optical test facility for determining the absorption of glass at melting temperatures. In: Proc. 5th Conf. European Society of Glass Science and Technology (ESG), Prague 1999. Vol. A5, p. 51–58. (Available on CD-ROM.)
[42] Patankar, S. V.: Numerical heat transfer and fluid flow. New York, NY: Hemisphere Publishing, 1980.

1299P001

Addresses of the authors:

R. R. Hayes, J. Wang, M. Q. McQuay, B. W. Webb
Mechanical Engineering Department, 435 CTB
Brigham Young University
Provo, UT 84602 (USA)

A. M. Huber
Ford Motor Company Glass Division
15000 North Commerce Drive
Dearborn, MI 48120-1225 (USA)